Neuropeptides, substrates and inhibitors of human dipeptidyl peptidase III, experimental and computational study - a new substrate identified

Zrinka Karačić[a#], Filip Šupljika[b#], Antonija Tomić[a], Lidija Brkljačić[a], Ana Tomašić Paić[a], Mirsada Ćehić[a] and Sanja Tomić[a]*

[#] – these authors contributed equally

* Corresponding author: Sanja Tomić, Division of Organic Chemistry and Biochemistry, Ruđer Bošković Institute, Bijenička cesta 54, 10000 Zagreb, Croatia, e-mail: Sanja.Tomic@irb.hr

[a] Ruđer Bošković Institute, Division of Organic Chemistry and Biochemistry, Bijenička cesta 54, 10000 Zagreb, Croatia

[b] Faculty of Food Technology and Biotechnology, Department of Chemistry and Biochemistry, Pierottijeva 6, 10000 Zagreb, Croatia

Authors' e-mails: zkaracic@irb.hr, fsupljika@pbf.hr, Antonija.Tomic@irb.hr, Lidija.Brkljacic@irb.hr, Ana.Tomasic.Paic@irb.hr, Mirsada.Cehic@irb.hr

ABSTRACT

Dipeptidyl peptidase III (DPP III) is a cytosolic, two-domain zinc-exopeptidase. It is widely distributed in mammalian tissues, where it is involved in the final steps of normal intracellular protein degradation. However, its pronounced affinity for some bioactive peptides (angiotensins, enkephalins, and endomorphins) suggests more specific functions such as blood pressure regulation and involvement in pain regulation.

In this work, we have investigated several different neuropeptides as potential substrates and inhibitors of human DPP III. The binding affinities and kinetic data determined by isothermal titration calorimetry, in combination with fluorimetric measurements of enzyme inhibition identified the hemorphin-related valorphin, tynorphin, S-tynorphin, and I-tynorphin as the most potent inhibitors of DPP III (actually slow substrates), whereas hemorphin-4 proved to be the best substrate of DPP III of all neuropeptides examined. In addition, we have shown that the neuropeptides valorphin, Leu-valorphin-Arg, and the opioid peptide β-casomorphin, derived from the digestion of the milk protein casein, are DPP III substrates.

The molecular modelling of selected peptides shows uniform binding to the lower domain β-strand residues of DPP III *via* peptide backbone atoms, but also previously unrecognized stabilizing interactions with conserved residues of the metal-binding site and catalytic machinery in the upper domain. The computational data helped explain the differences between substrates that are hydrolyzed effectively and those hydrolysed slowly by DPP III.

KEYWORDS: dipeptidyl peptidase III; neuropeptide; hemorphin-4; isothermal titration calorimetry (ITC); enzyme kinetics

1. INTRODUCTION

The causes of neuropathological disorders are numerous and most of them are poorly understood. One cause of neuropathological disorders is altered metabolism of neuropeptides, of which the endogenous opioid peptides (dynorphins, endorphins, enkephalins) are best described [1,2]. Since it has been shown that dipeptidyl peptidase III (DPP III, sometimes referred to as enkephalinase B [3]) can efficiently bind and hydrolyze Leu-enkephalin and several other widely used neuropeptides, a more detailed study of the interactions of DPP III with neuropeptides proved necessary.

DPP III (EC 3.4.14.4) is a two-domain zinc dependent exopeptidase and the sole member of the peptidase family M49 (according to the MEROPS database, http://www.merops.ac.uk) [4]. M49 family is characterised with two highly conserved motifs HEXXGH and EEXR(K)AE(D), that in human DPP III correspond to ^{450}HELLGH^{455} and ^{507}EECRAE^{512}. Histidine residues from the first motif and E508 coordinate the zinc ion, while E451 is catalytically indispensable because it is involved in proton transfer during peptide hydrolysis.

DPP III is found in almost all living organisms, where it hydrolyzes dipeptides from the unsubstituted N-terminus of its peptide substrates, usually three to eight amino acids long [4–9]. Distributed in various mammalian tissues, DPP III is preferentially localised in the cytosol, but also occurs in the membrane [6,7,10] and has been found in extracellular fluids [11]. Because of its broad substrate specificity, it is thought to contribute to the final steps of normal intercellular protein degradation. However, its marked affinity for the bioactive peptides angiotensins and enkephalins, suggests a more specific function such as blood pressure and pain regulation.

Already in 1982 Lee and Snyder [8] showed that DPP III from rat brain efficiently hydrolyses Leu-enkephalin and angiotensin II and *in vitro* studies showed that it interacts with a number of opioid peptides such as: enkephalins (Leu-enkephalin and Met-enkephalin) [8,12], endomorphins (endomorphin-1 and endomorphin-2) [12], α-melanocyte-stimulating hormone [13] and dynorphin A (1-8) [12], as well as some hemorphins (valorphin) [12] and exorphins (β-casomorphin). The interaction was shown as inhibition of hydrolysis of DPP III-preferred synthetic substrate analogues Arg_2-2-naphthylamide (Arg_2-2NA) and Arg-Arg-4-methoxy-2-naphthylamide. For Leu-enkephalin and endomorphin-1, kinetic data have shown that they serve as DPP III *in vitro* substrates [12].

Moreover, the high concentrations of DPP III in the rat spinal cord, where the enkephalin-synthesising neurons are located, and its high affinity (*in vitro*) for opioid peptides such as enkephalins and endomorphins suggest its role in the mammalian pain-regulatory system [12,14]. Sato *et al*. (2003) found that the activity of DPP III in cerebrospinal fluid of patients with pain differs from that of patients without pain [11]. In line with these data are findings of Thanawala *et al*. [15] suggesting DPP III as a potential target for pharmacological treatment of pain, and Buckley *et al*. [16] that the DPP3 gene is regulated differently in patients with CNBP (Chronic Neuropathic lower Back Pain) than in the normal population. In addition, the endogenous heptapeptide spinorphin and its truncated form tynorphin [17,18] have been found to inhibit DPP III peptidase activity, and Ueda *et al*. demonstrated that spinorphin can induce analgesia in mice [19].

Cruz-Diaz *et al*. have shown that angiotensin-(1-7) is hydrolyzed by DPP III in renal epithelial cells, where it exhibits renoprotective effects [20]. Since Ang-(1-7) has both antiproliferative and antiangiogenic activity this may explain the relationship between the activity of DPP III and the aggressiveness of tumors in human cells [21,22]. Jha *et al*. found elevated levels of angiotensin-related peptides in DPP III knock-out mice [23]. Finally, Pang *et al*. [24] showed a link between DPP III and the renin–angiotensin system (RAS) and thus possible use of DPP III in the treatment of hypertension.

It should also be noted that DPP III is involved in the regulation of oxidative stress and in the development of some cancers in humans, a case of protein moonlighting unrelated to its peptidase activity [21,22,25–28].

One of the possible reasons why DPP III processes different peptides is its flexibility, and thus the adaptability of its binding site to accommodate molecules of different sizes. Indeed, experimental (X-ray diffraction) [29,30] and theoretical (molecular dynamics simulations (MD)) [31–33] studies have shown the coexistence of at least two different forms of DPP III, the so-called open and closed forms with semi-closed conformers of DPP III being the most suitable for substrate recognition.

Although the DPP III substrate specificity is not precisely defined, a preference for (a) a positively charged, unmodified, N-terminus, (b) the ability of the substrate to form β-strand secondary structures [31], and (c) hydrophobic amino acid residues at the P1' position [13,34] (for the definition of peptide and enzyme subsites see Scheme S1 in Supplementary data)was observed.

Information on the biological functions of DPP III, related to the hydrolytic activity of this enzyme on bioactive peptides, is still insufficient. Recently, however, evidence has been accumulating that is consistent with the assumptions based on the above mentioned results obtained *in vitro*. The colocalization of DPP III and neuropeptides in the cells of the superficial laminae and the demonstrated efficiency of the enzyme in the degradation of opioids and some other families of neuropeptides suggest that DPP III may play a role in pain regulation [12,13,30,35,36]. Therefore, our study to determine the human DPP III catalytic efficiency for selected biologically active peptides could make a valuable contribution to the knowledge of its potential, previously unrecognized natural substrates. In the present work we considered 7 opioid peptides (Leu-enkephalin, endomorphin-2, β-neoendorphin, β–casomorphin, valorphin, Leu-valorphin-Arg, hemorphin-4), Arg-vasopressin from the vasopressin/oxytocin gene family, angiotensin II, endogenous brain peptide hemopressin and potent synthetic inhibitors of DPP III, tynorphin, S-tynorphin, and I-tynorphin. Cleavage of peptides by recombinant human DPP III was determined using HPLC-MS. The inhibitory effect on the action of the enzyme was determined following the hydrolysis of the fluorogenic synthetic substrate Arg_2-2NA. Isothermal titration calorimetry (ITC) was used to determine binding affinity, as well as kinetic parameters for selected peptides. Finally, the computational study allowed us to investigate subtle differences in the structure of the complexes of DPP III with substrates and, in this way, to explain the different catalytic efficiency of DPP III measured in relation to them.

2. MATERIALS AND METHODS

2.1 EXPERIMENTAL METHODS

2.1.1 Chemicals and consumables

Peptides were synthesized with purity > 98.0% as a commercial service by Pepmic Co. (China) (endomorphin-2, hemorphin-4, β-neoendorphin, I-tynorphin, S-tynorphin) and Proteogenix (France) (angiotensin II, tynorphin, valorphin), or by Huib Ovaa's group (Leiden, Netherlands) (endomorphin-2, hemorphin-4, Leu-valorphin-Arg, Arg-vasopressin, hemopressin, β-neoendorphin). Tris buffer, LB broth, ampicillin, isopropyl-ß-D-thiogalacto-pyranoside (IPTG), imidazole, NaCl, acrylamide/bisacrylamide solution (29:1), *N*,*N*,*N*',*N*'-tetramethylethylenediamine (TEMED), ammonium peroxide, Rotigarose His/Ni beads, methanol, and acetic acid were aquired from Carl Roth (Germany). Arg_2-2-naphthylamide (Arg_2-2NA) was produced by Bachem (Switzerland), 2-naphthylamine (2-NA), 2-mercaptoethanol, and DNase I from bovine pancreas by Merck (Germany). For visualisation of SDS-PAGE gels we used PhastGel Blue R tablets (Pharmacia, Sweden).

2.1.2 Recombinant protein expression and purification

Protein was produced as a full length Uniprot sequence (Q9NY33) with a His_6-tag at the C-terminus, by a standard affinity purification protocol. In short, the gene for human DPP III originally cloned from human cDNA into a pET21b plasmid [37] was expressed in BL21-CodonPlus (DE3)-RIL *E. coli* cells. Cells were initially grown for 2-3 hours at 37 °C at 220 rpm shaking. Induction was started at OD_{600} = 0.6 with 0.25 mM IPTG and bacteria were cultured at 18 °C and 120 rpm overnight, for approximately 20 hours. Bacterial cells were pelleted and frozen at -20 °C until use. Pellets were resuspended in lysis buffer (50 mM TrisHCl pH 8.0, 300 mM NaCl, 10 mM immidazole), treated with lysosyme for 30 minutes at 0 °C and sonicated in two 3 minute intervals (80 % amplitude, 2 s pulse, Ultrasonic processor, Cole Palmer, USA). The lysate was incubated for 20 minutes at room temperature with DNase I (Merck, Germany) and cleared by centrifugation for 45 minutes at 14500 g at 4 °C. His/Ni beads equilibrated with lysis buffer were used to capture the His-tagged human DPP III by a batch protocol. Beads were washed with wash buffer (same as lysis but 20 mM immidazole) and protein was eluted using elution buffer (same as lysis but 300 mM immidazole). Pooled fractions were desalted by dialysis (for ITC) or on a PD-10 column, depending on the amount of protein. Protein was concentrated on an Amicon Ultra 15 centrifugal filter with 30000 Da cutoff (Merck, Germany), purity was evaluated on SDS-PAGE [38], and aliquots were flash-frozen in liquid nitrogen and stored at -80 °C until use. The wild type protein was purified in two batches, one used for HPLC-MS and inhibition studies, another for ITC kinetics. ITC binding was perfomed with inactive mutant E451A, prepared using a mutagenesis Quikchange II kit (Agilent, USA), using primers: E451A_F GGTGGGCCTGCACGCGCTGCTGGGCCATG and E451A_R CATGGCCCAGCAGCGCGTGCAGGCCCACC, according to manufacturers' instructions. Full-length gene sequencing to confirm successful mutagenesis was done at Macrogen Europe (The Netherlands).

2.1.3 HPLC-MS experiments

For identification of human DPP III substrates, a simple LC-MS method was developed. MiliQ® water (18.2 MΩ cm^{-1}; purified by MiliQ water purification system (Millipore, USA)) and HPLC gradient-grade acetonitrile (J.T.Baker, USA) were used with analytical-grade formic acid (FA) (Acros Organics, Belgium) for mobile phase preparation. Stock solutions of peptides were prepared as 1-10 mM solutions in MiliQ water. To test whether the enzyme cleaves an individual peptide, two reactions were made for each selected peptide, sample (with enzyme) and blank (without enzyme). Peptide cleavage and enzyme activity was estimated by monitoring the decrease of the peptide signal area in the sample compared to the blank. Reaction mixures of 200 µL were prepared in 40 mM NH_4HCO_3 buffer pH = 7.4 with 0.18 µM enzyme and 1 mM peptide. Residual peptide was quantified after incubation for 15 min, 2 h or 24 h at room temperature. Reactions were stopped by addition of 100 µL of ACN for inhibition of enzyme activity and frozen until analysis. Samples were filtered and 5 µL of clear solution was injected on LC column. LC–MS analysis was carried out using an Agilent Technologies 1200 series HPLC system equipped with a binary pump, a vacuum membrane degasser, an automated autosampler and injector interfaced with 6420 triple quadropole mass spectrometer with electrospray ionization source (ESI) (Agilent Technologies Inc., USA). The analysis was performed on Zorbax XDP C18 column (75 x 4.6 mm, 3.5 µm particle size) (Agilent Technologies Inc., USA). Solvents for the analysis were 0.1% formic acid (FA) in water (solvent A) and acetonitrile (solvent B). The gradient was applied as follows: 0 min 90% A, 0-15 min 90% A-0% A, 15-17 min 0% A, 17.1-20 min 90% A. Flow rate was 0.5 mL/min. The electrospray ionization source was operated in a positive mode and samples were detected in the single ion monitoring (SIM) mode. Monitored *m*/*z* for each peptide and corresponding retention time is shown in Table S1 in Supplementary data. Fragmentor voltage for all peptides was set at 135 V. The desolvation gas temperature was 300 °C with

gas flow rate of 11.0 L/min. The capillary voltage was 4.0 kV. All data acquisition and processing were performed using Agilent MassHunter software.

2.1.4 Enzyme inhibition studies

Enzyme kinetics was measured with Arg_2-2NA as an artificial substrate analog, as previously described [30]. After hydrolysis, a fluorescent product, 2-NA, is released and detected. A calibration curve was determined with 2-NA on an Agilent Cary Eclipse fluorescence spectrophotometer (Agilent, USA). Reaction mixture contained 20 mM Tris HCl pH = 7.4, 0.25 – 100 µM Arg_2-2NA, and fixed concentrations of inhibitor, and was preincubated at 25 °C for 2 minutes. Reaction was started by addition of enzyme (final concentration 1 nM) and 2-NA release was measured during 1 min with extinction at 332 nm and emission at 420 nm with slit widths 10 and 5 nm, respectively. Rate of reaction was determined from the slope of intensity versus time. Care was taken that all reactions yielded a maximum of 5 % of product. Double-reciprocal graphs [39] were visualised to determine the type of inhibition. Experimental data was analysed in GraphPad 5 (GraphPad, USA) using global nonlinear regression and in-built pre-set analysis for competitive inhibition of enzymes (Michaelis-Menten kinetics). Inhibition of the enzyme reaction was measured at three different peptide concentrations for each peptide. K_i was expressed as best-fit value and standard error of nonlinear regression fit.

2.1.5 ITC binding experiments

Peptide binding to inactive human DPP III variant E451A was performed on a MicroCal PEAQ-ITC microcalorimeter (Malvern, UK). Peptide was dissolved and protein dialysed in the same batch of 20 mM Tris HCl buffer pH = 7.5. Further dilutions were made using the same buffer. Protein solution (80-150 µM) was in the cell (200 µL) and peptide solution (0.2-1.3 mM) was in the syringe (40 µL). Experiments to correct for heat of dilution (buffer-buffer, peptide-buffer, buffer-protein) were perfomed for all experiments. Measurements were made at 25 °C and 500 rpm strirring, with reference power set to 30 µW. The reaction was started with a 0.4 µL injection of peptide followed by 18 injections 2.0 µL each, with 180 seconds spacing to allow for equilibration. MicroCal PEAQ-ITC analysis software, supplied by the manufacturer, was used for data analysis. Affinity constant K_D, reaction enthalpy $\Delta_r H$, reaction Gibbs energy $\Delta_r G$ and entropy contribution $-T^*\Delta_r S$ were expressed as average value and standard deviation of at least three measurements.

2.1.6 ITC kinetic experiments

Calorimetric experiments to determine kinetic parameters experiments were performed on a MicroCal PEAQ-ITC microcalorimeter (Malvern, UK). MicroCal PEAQ-ITC analysis software, supplied by the manufacturer, was used for data analysis. Experiments were performed in 50 mM Tris-HCl buffer with 100 mM NaCl, pH = 8.0 at 25.0 °C, with 500 rpm strirring and reference power set to 30 µW. Two kinds of enzyme kinetics experiments were performed, single injection experiments (SIM) and multiple injection experiments (MIM). In SIM experiments there is a complete conversion of the substrate into the product, while in the MIM experiments there is a partial conversion of the substrate into the product (up to 5%) during each injection of substrate into the enzyme solution. SIM titrations were performed with all peptides, including slow substrates, while MIM titrations were performed only with hemorphin-4, Leu-enkephalin and Leu-valorphin-Arg. Typically, SIM titration was performed in a way that one aliquot of 5 µL of the peptide (c = 2 mM) was injected from rotating syringe (500 rpm) into the isothermal cell, equilibrated at 25.0 °C, containing 200 µL of human DPP III wt (c = 0.2 – 50 µM). The spacing was in the range 300-600 s and initial delay before first injection was 180 s. MIM titration was performed in a way that thirty-five aliquots of 1 µL of the peptide (c = 0.5 - 1 mM) were injected from rotating syringe (500 rpm) into the isothermal cell, equilibrated at 25.0 °C, containing 200 µL of human DPP III wt (c = 0.1 – 0.5

μM). The spacing between each injection as well as initial delay was 60 s. Obtained kinetic parameters K_M and k_{cat} as well as reaction enthalpy $\Delta_r H$ were expressed as average value and standard deviation of at least three measurements.

2.2 COMPUTATIONAL METHODS

2.2.1 Preparing complexes for MD simulations (System preparation)

To construct the initial complexes, the crystal structures of the inactive mutant E451A of human DPP III with tynorphin (PDB_id 3t6b), Leu–enkephalin (PDB_id 5e3a), and endomorphin-2 (PDB_id 5ehh) were used as templates. In all complexes the initial protein conformation corresponds to DPP III in the complex with tynorphin (PDB_id 3t6b) in which Ala451 is mutated back to Glu. Since this structure lacks the metal ion in the active site, the zinc ion was modelled using the DPP III – endomorphin-2 complex (PDB_id 5ehh), while the position of the ligands was as follows: Leu–enkephalin as in PDB file 5e3a, tynorphin as in PDB file 3t6b, the position of valorphin is based on the position of tynorphin, and the position of hemorphin-4 (YPWT) is based on the position of endomorphin-2 (YPFF) in PDB file 5ehh.

An alternative DPP III – valorphin complex was obtained with Autodock4, but since the substrate subsite P1 (see Scheme S1) in the selected complex with the lowest energy was in a position less suitable for hydrolysis than in the complex obtained with the crystal structures of human DPP III with tynorphin as template, we refrained from further simulations.

The position of a water molecule coordinating Zn^{2+} was determined in our previous QMMM study [35]. All Arg and Lys were positively charged, and Glu and Asp residues were negatively charged in the structures. The histidines were in a neutral state with a proton at the Nε atom, except histidines directly coordinating zinc ion (H450 and H455) which were Nδ protonated and H568 which was positively charged (both, Nε and Nδ protonated), as determined in our previous studies. Parametrization was performed using ff19SB force field [40] and for the zinc ion, the extended 4-ligand hybrid bonded/non-bonded parameters derived in our previous work were used [41]. The complexes were neutralised with Na^+ ions and solvated in an octahedral box filled with OPC water molecules [42] which were recommended to be used with the ff19SB force field [40]. The minimum distance between the solvated complex and the edge of the box was 11 Å. Solvated systems were minimized, followed by heating, density equalization, and productive MD simulations.

2.2.2 MD simulations details

All simulations were carried out using the AMBER20 suit of programs [43]. System minimization was performed in 3 cycles.

In the first cycle of optimization (1500 steps), water molecules were relaxed, while the rest of the system was harmonically restrained with a force constant of 32 kcal mol^{-1} $Å^{-2}$. In the second cycle (2500 steps), the protein and the peptide backbone atoms were restrained with a force constant of 12 kcal mol^{-1} $Å^{-2}$. In the third cycle (1500 steps), the force constant of the restrain applied to the protein and the peptide backbone atoms was reduced to 6 kcal mol^{-1} $Å^{-2}$. In case of valorphin, one additional minimization cycle (4500 steps) was conducted without any constrains. Minimizations were performed using 470 steps of steepest descent followed by the conjugated gradient for the remaining steps in each cycle.

The energy-optimized system was heated from 0 to 300 K during 30 ps using the NVT ensemble. Followed 970 ps of the solvent density equilibration using the NPT ensemble, which was performed in two steps, 470 ps and 500 ps long. The equilibrated systems were simulated 1 μs. During heating and equilibration,

the time step was 1 fs and during the productive MD simulations 2 fs. The SHAKE algorithm was used to constrain covalent bonds involving hydrogen atoms. The pressure was maintained at 1 atm with a pressure relaxation time of 1 ps using the Berendsen barostat [44], while the system temperature was kept constant at 300 K by the Langevin thermostat [45] with a collision frequency of 5 ps^{-1} (during heating and the 470 ps of equilibration) and 2 ps^{-1} (during the last 500 ps of equilibration and the productive MD simulations). Simulations were performed using periodic boundary conditions (PBC) with a cutoff value of 11 Å, while the particle mesh Ewald (PME) method was used to calculate the long-range electrostatic interactions.

Since the X-ray structure of DPP III with the penta-peptide tynorphin served as a template for the construction of the complex with the hepta-peptide valorphin, heating, equilibration of solvent density, and the first 50 ns of the production phase were carried out with the peptide residues at positions P2, P1 and P1', as well as the protein residues E316, Y318 and H568, harmonically restrained. During 30 ps of heating from 0 to 300 K using the NVT ensemble and 970 ps of the solvent density equilibration using the NPT ensemble aforementioned residues were harmonically restrained with a force constant of 32 kcal mol^{-1} $Å^{-2}$. The equilibrated systems were gradually relaxed during a series of 5 10-ns-long productive MD simulations applying a harmonic restrain with a force constant of 32 kcal mol^{-1} $Å^{-2}$ for the following residues: 1) all atoms of the above mentioned residues, 2) the peptide residues P2, P1 and P1' as well as the backbone atoms of E316, Y318 and H568, 3) and 4) the peptide residues P2, P1 and P1', and 5) only the backbone atoms of the peptide residues P2, P1 and P1'. In this way, the H-bonds network important for the binding of the peptide residues P2, P1' and P1 to the lower protein domain was preserved. The next 1 μs of productive MD simulation was conducted without any constraints utilizing the same conditions as for other studied peptides.

2.2.3 MM/PBSA and residue based MM/GBSA calculations

The peptide binding free energies were approximated by MM/PBSA (Molecular Mechanics Poisson-Boltzmann Surface Area) [46] energies calculated within AMBER20 program. For each complex the MM/PBSA energies have been calculated on a set of 10 equally distributed 20-ns-long time intervals (1000 evenly spaced snapshots per interval) sampled throughout simulations using a single trajectory approximation. Calculations were performed for the enzyme with dielectric constant 2.0 immersed in the solvent with dielectric constant 80. The ion concentration was 0.02 M. The polar component of the enthalpy of solvation was calculated by the Poisson-Boltzmann method, and the nonpolar component was determined by $\Delta H_{nonpol} = \gamma SASA + \beta$, where the surface area accessible by the solvent (SASA) was calculated using the MolSurf program [47]. The surface tension γ and the offset β were set to the standard values of 0.0378 kcal $(mol\ Å^2)^{-1}$ and 0.5692 kcal mol^{-1}, respectively. The zinc charge was +1.21 e.

To elucidate the differences in binding energies and identify the residues critical for ligand binding, the free energy of binding between the protein and the peptide was decomposed into the contribution of each residue using the MM/GBSA (Molecular Mechanical Generalized Born Surface Area) approach implemented in the AMBER20 software. Residue-based MM/GBSA free energy analysis was performed to highlight the residues relevant to the stabilization of the ligand. Calculations were performed for the enzyme with a relative permittivity of 1.0 immersed in a solvent with a relative permittivity of 80.0. MM/GBSA calculations were performed for the last 0.6 μs of the MD simulations (from 400^{th} to 1000^{th} ns) under NPT conditions, sampling the structures every 100 ps.

We calculated the contribution of enthalpy to binding free energy, since conformational entropy is usually neglected due to its high computational cost when only the relative binding free energies of similar ligands are needed.

2.2.4 Geometrical data analysis

Box plot diagrams were made in program Origin 7.0 (https://www.originlab.com/) on the data (distances and angles) derived from MD simulations by cpptraj module. Diagrams represent summary statistics as the box is defined by the 25th and 75th percentiles, while the whiskers depict the standard deviation. Origin's box chart also includes the minimum, median, mean, maximum and 1st and 99th percentiles.

3. RESULTS & DISCUSSION

3.1 Experimental results

We produced wild-type of hDPP III to identify peptides this enzyme cleaves and peptides that inhibit it. Inactive variant E451A was produced to quantify binding affinity of neuropeptides to hDPP III. Purified protein samples were visualized using SDS-PAGE and estimated to be 90 % homogenous and sufficiently pure for planned experiments (see Figure S1., Supplementary data).

3.1.1 HPLC-MS results / Peptide degradation

Peptide degradation was measured by HPLC-MS quantification of the peptide remaining in the reaction mixture after incubation with the enzyme for 2 and 24 hours. For Arg-vasopressin, hemopressin, and β-neoendorphin, neither degradation nor cleavage products were detected. All other peptides were cleaved by human DPP III (Table 1). For more details see Supplementary data, Table S1 and Fig. S2.

It is not surprising that human DPP III does not cleave Arg-vasopressin because it has a disulfide bridge between cysteines in the first and sixth positions and appears unusual as a substrate. Hemopressin, a nonapeptide that has no sequence similarity to known DPP III substrates, is also not cleaved. Because RVD- and VD-hemopressin, endogenous versions of this peptide, are longer than 10 amino acids, we assumed that they are also not substrates of DPP III and were therefore not included in our screening. However, β-neoendorphin, whose first five amino acids are identical to Leu-enkephalin, is not cleaved, which surprised us. All other peptides, three hemorphins (hemorphin-4, valorphin, and Leu-valorphin-Arg), β-casomorphin, and tynorphins previously shown to be inhibitors of DPP III, were confirmed as substrates. Hemorphin-4 has not been tested previously, whereas the results for the other compounds are consistent with previous reports [48].

3.1.2 Enzyme inhibition

K_i was determined as the constant of inhibition of Arg_2-2NA cleavage by human DPP III at three different peptide concentrations (Table 1). All peptides that inhibited the reaction behaved as competitive inhibitors (Fig. S3). Three peptides that were not cleaved by DPP III: Arg-vasopressin, hemopressin, and β-neoendorphin, did not inhibit the enzyme in the range of peptide concentrations tested from 1 to 50 μM (data not shown).

Our results confirm that I-tynorphin is the most potent peptide inhibitor of human DPP III, with an inhibitory constant in the subnanomolar range. This is consistent with the measurements of Chiba *et al*. for DPP III from rat brain [14]. However, their measurements predicted that tynorphin is a stronger inhibitor than S-tynorphin, in contrast to our measurements where tynorphin is a weaker inhibitor of human DPP III than S-tynorphin. While they described all tested peptides as noncompetitive inhibitors, we have shown that they are competitive inhibitors. The latter makes more sense, because there are X-ray structures of the peptide bound in the substrate binding site of the enzyme. Breinbauer *et al*. also

showed that DPP III cleaves tynorphin, albeit in a slower reaction [49]. Moreover, no additional binding or allosteric site has yet been identified in DPP III. Valorphin, like tynorphin and its derivatives, is a potent inhibitor of DPP III, with K_i in the low nM range, as previously reported. This result could be explained by sequence similarity since valorphin is only two amino acids longer than tynorphin at the C-terminus. For all other peptides, the determined K_i was in the low μM range, with β-casomorphin between the two groups. Our data agree well with previously published data [12].

3.1.3 Binding affinity

Thermodynamic data obtained by ITC measurements are given in Table 2. For endomorphin-2, Leu-enkephalin, and ß-casomorphin, we determined K_d but were unable to obtain a complete titration curve due to the low *c* - value (Fig. S4). All other peptides showed endothermic, entropy-driven binding (Figs. 1 and S4). Arg-vasopressin, hemopressin and β-neoendorphin did not bind to the inactive human DPP III, confirming our findings that they are neither substrates nor inhibitors of human DPP III.

The endothermic, entropy-driven thermodynamic signature of binding to DPP III is one of its specific features, related to the structure of the enzyme, as two domains move relative to each other, opening and closing the cleft to which the substrate binds [29,30,49–51]. To date, only two cases of exothermic binding have been reported: for a synthetic compound that binds to human DPP III [50], and for angiotensin II binding to a DPP III homolog from *Porphyromonas gingivalis* [51]. For the peptides that do not show binding to the inactivated enzyme, we have supporting data from HPLC-MS measurements and enzyme inhibition studies confirming that these peptides do not interact with human DPP III (see Table 1). The trend of K_d values is consistent with that of K_i values and differs only for β-casomorphin. β-Casomorphin had the highest measured K_d, followed by Leu-enkephalin, endomorphin-2 and hemorphin-4. However, there is a significant discrepancy between our data for Leu-enkephalin, for which we measured a K_d value of 118 μM, and the data reported by Bezerra *et al*. with a K_d value of 3.5 μM. This might be due to a buffer effect, as we measured binding affinities in 20 mM Tris-HCl buffer pH = 7.5, whereas Bezerra *et al*. used 50 mM Tris-HCl buffer pH = 8.0 with additional 100 mM NaCl. (We later switched to this buffer for kinetic measurements using ITC because we measured significant contributions of peptide dilution when it was dissolved in our first buffer. The difference might be attributed to different ionic strength of buffers.) Tynorphin and its derivatives are strong binders with a K_d in the nanomolar range, as measured previously: 0.44 μM K_d for tynorphin [29] agrees well with our 0.39 μM, as does 0.23 μM for I-tynorphin [30] with our 0.098 μM. Valorphin has a similar sequence to tynorphin but does not bind just as well and has a micromolar K_d value. Leu-valorphin-Arg, only two amino acids longer than valorphin, has a similar dissociation constant K_d but a much higher K_i. Our data on angiotensin II are also consistent with previously published values: 2.22 μM K_d versus 1.64 μM [30].

3.1.4 Enzyme kinetics using ITC

To determine the kinetic parameters of peptide cleavage by DPP III, we wanted to use HPLC-MS, but the method was not precise enough. Therefore, we resorted to the ITC method, which had been used previously for the same purpose [23]. Kinetic data were determined for Leu-enkephalin, hemorphin-4, and Leu-valorphin-Arg (Table 3, Fig. 2), using both SIM (in triplicate) and MIM measurements (Table S2) to confirm the SIM data. All other tested peptides showed „slow substrate“ behaviour, a profile that could not be analysed (Figs. 2 and S5).

We were able to measure the kinetic parameters of Leu-valorphin-Arg cleavage, but they were low. This is consistent with the general trend of our data, which suggests that hemorphin peptides are slow substrates. The hemorphin-related peptides can be ranked in order: I-tynorphin, S-tynorphin, tynorphin, valorphin, and Leu-valorphin-Arg, according to increasing inhibition and dissociation constants. The ITC

data for these substrates show an endothermic contribution to the curve followed by an exothermic one. Here we see the endothermic effect of peptide binding, which is not observed for other substrates. All slow substrates have been shown to be cleaved by human DPP III, but the reason for the lower reaction rates is unknown, possibly due to the strong binding of their products, trapping the enzyme in a non-productive conformation [36], or due to other differences in the hydrolysis mechanism [30]. However, hemorphin-4 showed the highest k_{cat} of all peptides. It is also the only DPP III substrate in our screen that has not been previously tested, as either DPP III substrate or an inhibitor. The values measured for hemorphin-4 (inhibition constant, binding affinities) are similar to those of Leu-enkephalin and endomorphin-2, also opioid peptides, previously shown to be substrates of human DPP III, therefore suggesting that hemorphin-4 is also an *in vivo* substrate of human DPP III. β-Casomorphin on the other hand, does not fit neatly into Table 1. It binds poorly but is a fairly good inhibitor, suggesting that it has a slow turnover, and a different mechanism of inhibiting the enzyme than tynorphins.

Our K_M values are all somewhat higher than those previously reported [12,23], but the k_{cat} values are in the same range. We measured the highest k_{cat} value for hemorphin-4. It is in the same range as the values measured for endomorphin-1 and Leu-enkephalin [12], and higher than the value measured for angiotensin II and its derivatives [23].

3.2 Computational study

The experimental approach used in this work identified *in vitro* substrates of DPP III. The details of the peptide-enzyme interactions were determined using an *in silico* approach. Computational studies were performed for two slow substrates, tynorphin and valorphin, and two substrates which are effectively cleaved by DPP III, Leu-enkephalin and hemorphin-4. Complexes were built using the experimentally determined structures of DPP III with tynorphin, Leu-enkephalin and endomorphin-2 as templates (see Section 2.2.1.). The solvated complexes were minimized and equilibrated, and two 1 μs MD simulations were performed for each (referred to as A and B in the Supplementary data).

The overall structure of the protein and the binding of substrates to the β-strand of the lower protein domain were maintained in most simulations (Figs. S6 – S7). In the case of the DPP III – valorphin complex, the MM/PBSA energies are similar in both simulations, whereas they differ significantly (vary in a range of almost 20 kcal/mol, Fig. S8) in the case of the Leu-enkephalin and tynorphin. During one simulation of hemorphin-4 (simulation B, Fig. S8) large fluctuations in MM/PBSA energies were observed. Interestingly, in the simulations with the low binding energies and the small fluctuations in the energies, the changes in protein compactness were insignificant, whereas in the simulations where protein compactness decreased significantly, the binding free energies were higher and fluctuated more (Figs. S6 and S8).

In the simulations where the protein compactness decreased, the volume of the enzyme active site increased and more water molecules entered into the interdomain cleft (Figs. S9 and S10). As a result, the network of hydrogen bonds, mainly between the protein and ligand's P2-P1-P1' residues in the case of hemorphin-4, and P2'-P3' residues in the case of Leu-enkephalin, was partially disrupted and the interactions between them weakened (Fig. S11). Consequently, the ligand binding energies determined in these simulations are less favourable than the energies determined in simulations where the ligand was more tightly bound in the protein (Fig. S8).

Since the systems with lower enthalpies are more populated and thus more relevant, we focused further analysis on the simulations with lower MM/PBSA energies (Fig. 3). In the case of valorphin (similar MM/PBSA energies), which according to experimental results is a slow substrate of DPP III like tynorphin, we focus our analysis mainly on the results of the MD simulation in which the valorphin orientation in the active site of the enzyme is similar to the orientation of tynorphin (Fig. S12).

In all low-energy simulations, the peptides were bound in an antiparallel orientation to the β-strand from the lower domain of the enzyme and formed H-bonds *via* the backbone atoms with the residues of the β-strand throughout the simulation while interacting specifically with the amino acid residues from the upper protein domain. (Fig. 4 and Fig. S7).

MM/GBSA decomposition analysis together with hydrogen bonding analysis revealed protein-ligand interactions important for ligand stabilization (Figs. 5 and 6).

Overall, the highest stabilization was found for aromatic residues. Tyrosine at position P2 in Leu-enkephalin and hemorphin-4, tryptophan in hemorphin-4 and tyrosine in valorphin and tynorphin at position P1', phenylalanine at position P2' of Leu-enkephalin and tryptophan at position P3' in tynorphin and valorphin (Fig. 5).

The residue-base MM/GBSA energy decomposition analysis shown in Fig. 6. indicates that most of the protein residues participating in ligand stabilization (with energy above ±1.5 kcal/mol) are the ones from protein S2, S1 and S1' subsites, interacting with ligand P2, P1 and P1' residues. The ligand residues at the P2' position are significantly stabilized only by Ala416, Arg669, Phe443, Arg572, and Arg548.

MM/GBSA analysis performed 'per protein residues' identified A388, G389, H450 and E512 as residues contributing most to the stabilization of the ligand P1' subsite. With the backbone of A388 and G389, the peptides form nonspecific hydrogen bonds, while they interact specifically with the side chains of H450 and E512. The aromatic residues in the position P1' form stacking interactions with H450 and hydrogen bonds with E512 (Fig. 4 a, b, and d). H450 and E512 are 100 % conserved residues that form the first and second coordination spheres of the zinc ion and belong to the upper protein domain. The other 100% conserved histidine (H455) coordinating zinc ion interacts with the aromatic residues at the P2 position of hemorphin-4 and Leu-enkephalin also through stacking interactions. As already observed, ligand N-terminus is anchored in the enzyme active site by numerous hydrogen bonds with Glu316, Asn391 and Asn394. Slightly lower energy contributions (lower than −5 kcal/mol) are observed for Tyr318, Pro387 Ile390 and Glu508 residues that mostly participate in ligand P1 residue stabilization.

The residue-based MM /GBSA energies for the tripeptide (P2-P1-P1') at the N-terminus of the substrates, adjacent to the cleavable peptide bond, indicate the best overall stabilization for hemorphin-4, which is mainly a consequence of more specific interactions of the ligand side chains with the upper domain residues of the protein (the largest contribution comes from H450, H455, and E512).

Tighter binding with the upper domain residues of the protein was also observed during Leu-enkephalin hydrolysis, as shown in our previous publication [36]. We hypothesize that this prevents the formation of a stable (low energy) intermediate observed during tynorphin hydrolysis, and thus promotes the forward reaction leading to a final product. All of this provides an explanation for the highest k_{cat} measured for hemorphin-4 compared to the k_{cat} values determined for the other peptides.

The stabilization of the C-terminus of tynorphin and Leu-enkephalin by Arg669 observed in our previous work [36] was also observed in this study, as was the stabilization of the P3' residue of valorphin whose C-terminus (P5' residue) is strongly stabilized by another arginine, R548. Both tryptophan (tynorphin and valorphin) and leucine (Leu-enkephalin) at the P3' position (C-terminus) form salt bridge or hydrogen bond interactions with R669; in addition, the indol group of tryptophan makes cation-π interactions with R669 and the isobutyl group of leucine makes numerous van der Waals interactions with amino acid residues of the upper protein domain (e.g. Phe 443, see Figs. 4c and 6). The significant stabilization of R669 in complex with Leu-enkephalin is also due to its cation-π interactions with the aromatic ring of the phenyalanine residue at the P2' position. Overall, residues away from the cleavable peptide bond toward the C-terminus (P2'-P'n) of the slow substrates tynorphin and valorphin are strongly stabilized by amino

acid residues from both protein domains. This is consistent with the strong stabilization of the products of tynorphin hydrolysis preventing revitalization of the enzyme. Since the MD simulations revealed higher fluctuations in the number of water molecules in the 1st solvation sphere of the ligand as well as in the number of protein-ligand hydrogen bonds in the case of valorphin than in the case of tynorphin (Figs. S10 and S11), this might be the reason why tynorphin is a better inhibitor of DPP III compared to valorphin. In addition, the energy calculated by averaging the MM/PBSA energies for the two 1 μs-long trajectories is lowest for tynorphin (ΔH = −15.5 kcal/mol), suggesting that tynorphin binds most strongly, whereas binding of the other three substrates is similarly strong (approximately −10 kcal/mol) (Fig. S8).

The simulations showed that in all complexes at least one zinc-coordinated water molecule is hydrogen-bonded to E451 throughout the simulations (Fig. S13) so that it can be easily activated and attack the carbonyl carbon of the second (P1-P1') peptide bond to perform the first step of peptide hydrolysis. Interestingly, the shortest average distances between the catalytic zinc ion and the carbonyl oxygen of the cleavable peptide bond (Fig 7a), and oxygen atom of the activated water molecule and carbonyl carbon of the cleavable peptide bond (Fig 7b) are determined for the complexes with hemorphin-4 and Leu-enkephalin, the peptides most effectively cleaved by DPP III (Figs. 7 and S14). In addition, MD simulations showed that the angle indicating the direction for nucleophilic addition of the OH^- ion is closer to Bürgi–Dunitz angle of about 107° [52] during simulations with hemorphin-4 and Leu-enkephalin (Figs. 7c and S15) which further explains why they are better substrates of DPP III than hemorphin-related peptides.

On the basis of the ligand binding modes identified here, we can hypothesize that the reason why hemopressin and β-neoendorphin are not cleaved by DPP III (as shown in Table 1) is that, when bound in the mode appropriate for hydrolysis, their positively charged residues (Arg or Lys) at positions P3' (hemopressin) and P4' and P5' (β-neoendorphin) would interact with enzyme subregions rich in Arg residues, so-called Arg-anchors (e.g. R548, R572, and R669). These unfavourable interactions would probably prevent ligand binding in a way suitable for hydrolysis.

4. CONCLUSIONS

In this work, we investigated the efficiency of DPP III to catalyze the hydrolysis of several neuropeptides and the ability of these peptides to inhibit its enzymatic activity.

Using four different experimental methods, we identified valorphin, Leu-valorphin-Arg, β-casomorphin, and hemorphin-4 as *in vitro* substrates of human DPP III. The computational analysis performed for two good substrates, Leu-enkephalin and hemorphin-4, and two slow substrates, valorphin and tynorphin, showed that the good substrates are positioned more suitably for hydrolysis than slow substrates. Based on these new findings and the results of our previous study [36], it can be explained why Leu-enkephalin and hemorphin-4 are effectively cleaved by DPP III, and why the highest k_{cat} value was measured for hemorphin-4.

In agreement with previous results, our ITC measurements of K_d showed that the non-covalent binding of neuropeptides to DPP III is an entropy-driven process, with the largest contribution to entropy coming from water.[29,33]. In our MD simulations, the fluctuations in the number of water molecules in the 1st solvation sphere of the ligand and the number of protein-ligand hydrogen bonds was lower for tynorphin than for valorphin, which might explain the relative contribution of entropy change to experimentally determined binding affinity of these peptides. In addition, the energy calculated by averaging the MM/PBSA energies for the two 1 μs-long trajectories is lowest for tynorphin, suggesting that tynorphin binds most strongly. That agrees well with the experimentally determined binding affinity (ITC measurements) and inhibitory potency of the peptides, which indicated tynorphin as the strongest

inhibitor of human DPP III among these four simulated peptides. This approach, using experimental methods in combination with molecular modelling to characterise potential substrate of human DPP III, allowed us to obtain a wealth of data on the enzyme and to identify a new potential *in vivo* substrate of this enzyme, hemorphin-4.

CRediT authorship contribution statement

Zrinka Karačić: Conceptualization, Formal analysis, Investigation, Methodology, Validation, Visualization, Writing - original draft, Writing - review & editing.

Filip Šupljika: Formal analysis, Investigation, Methodology, Validation, Visualization, Writing - original draft, Writing - review & editing.

Antonija Tomić: Conceptualization, Data curation, Formal analysis, Funding acquisition, Investigation, Methodology, Validation, Visualization, Writing - original draft, Writing - review & editing.

Lidija Brkljačić: Investigation, Methodology, Visualization.

Ana Tomašić Paić: Investigation.

Mirsada Ćehić: Investigation.

Sanja Tomić: Conceptualization, Data curation, Formal analysis, Funding acquisition, Investigation, Methodology, Project administration, Resources, Supervision, Validation, Visualization, Writing - original draft, Writing - review & editing.

DECLARATIONS OF INTEREST: none

ACKNOWLEDGEMENTS

This work has been fully supported by Croatian Science Foundation under the project IP-2018-01-2936 and was partially funded by Foundation of the Croatian Academy of Sciences and Arts under Project Investigation of the peptidase activity of human DPP III against tynorphin—computational and experimental study.We are grateful to Huib Ovaa's group in Leiden, The Netherlands for the generous gift of peptide synthesis for initial screening.

REFERENCES

[1] L.D. Fricker, E.B. Margolis, I. Gomes, L.A. Devi, Five decades of research on opioid peptides: Current knowledge and unanswered questions, Mol. Pharmacol. 98 (2020) 96–108. https://doi.org/10.1124/MOL.120.119388.

[2] K. Kaczyńska, P. Wojciechowski, Non-opioid peptides targeting opioid effects, Int. J. Mol. Sci. 22 (2021) 13619. https://doi.org/10.3390/ijms222413619.

[3] A.J. Barrett, J.M. Chen, Dipeptidyl-peptidase III, in: Handb. Proteolytic Enzym. Third Ed., Elsevier Ltd, 2013: pp. 1285–1289. https://doi.org/10.1016/B978-0-12-079611-3.50247-0.

[4] J.M. Chen, A.J. Barrett, Dipeptidyl-peptidase III, in: Handb. Proteolytic Enzym. Second Ed., Academic Press, 2004: pp. 809–812. https://doi.org/10.1016/B978-0-12-079611-3.50247-0.

[5] S. Ellis, J.M. Nuenke, Dipeptidyl arylamidase III of the pituitary. Purification and characterization., J. Biol. Chem. 242 (1967) 4623–4629.

[6] Y. Inaoka, H. Tamaoki, Purification and characterization of enkephalinase B from rat brain membrane., Biochim. Biophys. Acta 925 (1987) 27–35.

[7] I. Ohkubo, Y.H. Li, T. Maeda, Y. Yamamoto, T. Yamane, P.G. Du, K. Nishi, Dipeptidyl peptidase III from rat liver cytosol: purification, molecular cloning and immunohistochemical localization., Biol. Chem. 380 (1999) 1421–1430. https://doi.org/10.1515/BC.1999.182.

[8] C.M. Lee, S.H. Snyder, Dipeptidyl-aminopeptidase III of rat brain. Selective affinity for enkephalin and angiotensin, J. Biol. Chem. 257 (1982) 12043–12050.

[9] M. Smyth, G. O'Cuinn, Dipeptidyl aminopeptidase III of guinea-pig brain: specificity for short oligopeptide sequences., J. Neurochem. 63 (1994) 1439–1445.

[10] J.K. McDonald, Dipeptidyl-peptidase III, in: A.J. Barrett, N.D. Rawlings, J.F. Woessner (Eds.), Handb. Proteolytic Enzym., Academic Press, London, 1998: pp. 536–8.

[11] H. Sato, K. Kimura, Y. Yamamoto, T. Hazato, Activity of DPP III in human cerebrospinal fluid derived from patients with pain, Japanese J. Anesthesiol. 52 (2003) 257–263.

[12] M. Baršun, N. Jajčanin, B. Vukelić, J. Špoljarić, M. Abramić, Human dipeptidyl peptidase III acts as a post-proline-cleaving enzyme on endomorphins, Biol. Chem. 388 (2007) 343–348. https://doi.org/10.1515/BC.2007.039.

[13] M. Abramić, M. Zubanović, L. Vitale, Dipeptidyl Peptidase III from Human Erythrocytes1. Abramić, M.; Zubanović, M.; Vitale, L. Dipeptidyl Peptidase III from Human Erythrocytes. Biol. Chem. Hoppe. Seyler. 1988, 369, 29–38, doi:10.1515/bchm3.1988.369.1.29., Biol. Chem. Hoppe. Seyler. 369 (1988) 29–38. https://doi.org/10.1515/bchm3.1988.369.1.29.

[14] T. Chiba, Y.H. Li, T. Yamane, O. Ogikubo, M. Fukuoka, R. Arai, S. Takahashi, T. Ohtsuka, I. Ohkubo, N. Matsui, Inhibition of recombinant dipeptidyl peptidase III by synthetic hemorphin-like peptides, Peptides 24 (2003) 773–778. https://doi.org/10.1016/S0196-9781(03)00119-0.

[15] V. Thanawala, V. Kadam, R. Ghosh, Enkephalinase Inhibitors: Potential Agents for the Management of Pain, Curr. Drug Targets 9 (2008) 887–894. https://doi.org/10.2174/138945008785909356.

[16] D.A. Buckley, E.M. Jennings, N.N. Burke, M. Roche, V. McInerney, J.D. Wren, D.P. Finn, P.C. McHugh, The Development of Translational Biomarkers as a Tool for Improving the Understanding, Diagnosis and Treatment of Chronic Neuropathic Pain, Mol. Neurobiol. 55 (2018) 2420–2430. https://doi.org/10.1007/s12035-017-0492-8.

[17] K. Nishimura, T. Hazato, Isolation and identification of an endogenous inhibitor of enkephalin-degrading enzymes from bovine spinal cord, Biochem. Biophys. Res. Commun. 194 (1993) 713–719. https://doi.org/10.1006/bbrc.1993.1880.

[18] Y. Yamamoto, J.I. Hashimoto, M. Shimamura, T. Yamaguchi, T. Hazato, Characterization of tynorphin, a potent endogenous inhibitor of dipeptidyl peptidaseIII, Peptides 21 (2000) 503–508. https://doi.org/10.1016/S0196-9781(00)00174-1.

[19] H. Ueda, S. Matsunaga, M. Inoue, Y. Yamamoto, T. Hazato, Complete inhibition of purinoceptor agonist-induced nociception by spinorphin, but not by morphine, Peptides 21 (2000) 1215–1221. https://doi.org/10.1016/S0196-9781(00)00262-X.

[20] N. Cruz-Diaz, B.A. Wilson, N.T. Pirro, K.B. Brosnihan, A.C. Marshall, M.C. Chappell, Identification of dipeptidyl peptidase 3 as the Angiotensin-(1–7) degrading peptidase in human HK-2 renal epithelial cells, Peptides 83 (2016) 29–37. https://doi.org/10.1016/j.peptides.2016.06.005.

[21] Š. Šimaga, D. Babić, M. Osmak, J. Ilić-Forko, L. Vitale, D. Miličić, M. Abramić, Dipeptidyl peptidase III in malignant and non-malignant gynaecological tissue, Eur. J. Cancer 34 (1998) 399–405. https://doi.org/10.1016/S0959-8049(97)00401-2.

[22] Š. Šimaga, D. Babić, M. Osmak, M. Šprem, M. Abramić, Tumor cytosol dipeptidyl peptidase III activity is increased with histological aggressiveness of ovarian primary carcinomas, Gynecol. Oncol. 91 (2003) 194–200. https://doi.org/10.1016/S0090-8258(03)00462-1.

[23] S. Jha, U. Taschler, O. Domenig, M. Poglitsch, B. Bourgeois, M. Pollheimer, L.M. Pusch, G. Malovan, S. Frank, T. Madl, K. Gruber, R. Zimmermann, P. Macheroux, Dipeptidyl peptidase 3 modulates the renin-angiotensin system in mice, J. Biol. Chem. 295 (2020) 13711–13723. https://doi.org/10.1074/jbc.RA120.014183.

[24] X. Pang, A. Shimizu, S. Kurita, D.P. Zankov, K. Takeuchi, M. Yasuda-Yamahara, S. Kume, T. Ishida, H. Ogita, Novel Therapeutic Role for Dipeptidyl Peptidase III in the Treatment of Hypertension, Hypertension 68 (2016) 630–641. https://doi.org/10.1161/HYPERTENSIONAHA.116.07357.

[25] H.-L. Chou, C.-T. Yao, S.-L. Su, C.-Y. Lee, K.-Y. Hu, H.-J. Terng, Y.-W. Shih, Y.-T. Chang, Y.-F. Lu, C.-W. Chang, M.L. Wahlqvist, T. Wetter, C.-M. Chu, Gene expression profiling of breast cancer survivability by pooled cDNA microarray analysis using logistic regression, artificial neural networks and decision trees, BMC Bioinformatics 14 (2013) 100. https://doi.org/10.1186/1471-2105-14-100.

[26] B.E. Hast, D. Goldfarb, K.M. Mulvaney, M.A. Hast, P.F. Siesser, F. Yan, D.N. Hayes, M.B. Major, Proteomic analysis of ubiquitin ligase KEAP1 reveals associated proteins that inhibit NRF2 ubiquitination, Cancer Res. 73 (2013) 2199–2210. https://doi.org/10.1158/0008-5472.CAN-12-4400.

[27] M. He, D.P. Mangiameli, S. Kachala, K. Hunter, J. Gillespie, X. Bian, H.-C.C.J. Shen, S.K. Libutti, Expression signature developed from a complex series of mouse models accurately predicts human breast cancer survival, Clin. Cancer Res. 16 (2010) 249–259. https://doi.org/10.1158/1078-0432.CCR-09-1602.

[28] K. Lu, A.L. Alcivar, J. Ma, T.K. Foo, S. Zywea, A. Mahdi, Y. Huo, T.W. Kensler, M.L. Gatza, B. Xia, NRF2 induction supporting breast cancer cell survival is enabled by oxidative stress-induced DPP3-KEAP1 interaction, Cancer Res. 77 (2017) 2881–2892. https://doi.org/10.1158/0008-5472.CAN-16-2204.

[29] G.A. Bezerra, E. Dobrovetsky, R. Viertlmayr, A. Dong, A. Binter, M. Abramic, P. Macheroux, S. Dhe-Paganon, K. Gruber, Entropy-driven binding of opioid peptides induces a large domain motion in human dipeptidyl peptidase III, Proc. Natl. Acad. Sci. 109 (2012) 6525–6530. https://doi.org/10.1073/pnas.1118005109.

[30] P. Kumar, V. Reithofer, M. Reisinger, S. Wallner, T. Pavkov-Keller, P. Macheroux, K. Gruber, Substrate complexes of human dipeptidyl peptidase III reveal the mechanism of enzyme inhibition, Sci. Rep. 6 (2016) 23787. https://doi.org/10.1038/srep23787.

[31] A. Tomić, S. Tomić, Hunting the human DPP III active conformation: Combined thermodynamic

and QM/MM calculations, Dalt. Trans. 43 (2014) 15503–15514. https://doi.org/10.1039/c4dt02003k.

[32] A. Tomić, M. Berynskyy, R.C. Wade, S. Tomić, Molecular simulations reveal that the long range fluctuations of human DPP III change upon ligand binding, Mol. BioSyst. 11 (2015) 3068–3080. https://doi.org/10.1039/C5MB00465A.

[33] A. Tomić, M. González, S. Tomić, The large scale conformational change of the human DPP III-substrate prefers the “closed” form, J. Chem. Inf. Model. 52 (2012) 1583–1594. https://doi.org/10.1021/ci300141k.

[34] I. Schechter, A. Berger, On the size of the active site in proteases. I. Papain, Biochem. Biophys. Res. Commun. 27 (1972) 157–162. https://doi.org/10.1016/0006-291X(72)90076-9.

[35] A. Tomić, B. Kovačević, S. Tomić, Concerted nitrogen inversion and hydrogen bonding to Glu451 are responsible for protein-controlled suppression of the reverse reaction in human DPP III, Phys. Chem. Chem. Phys. 18 (2016) 27245–27256. https://doi.org/10.1039/C6CP04580D.

[36] A. Tomić, S. Tomić, Demystifying DPP III Catalyzed Peptide Hydrolysis—Computational Study of the Complete Catalytic Cycle of Human DPP III Catalyzed Tynorphin Hydrolysis, Int. J. Mol. Sci. 23 (2022). https://doi.org/10.3390/ijms23031858.

[37] J. Špoljarić, B. Salopek-Sondi, J. Makarević, B. Vukelić, D. Agić, Š. Šimaga, N. Jajčanin-Jozić, M. Abramić, Absolutely conserved tryptophan in M49 family of peptidases contributes to catalysis and binding of competitive inhibitors, Bioorg. Chem. 37 (2009) 70–76. https://doi.org/10.1016/j.bioorg.2009.03.002.

[38] U.K. Laemmli, Cleavage of structural proteins during the assembly of the head of bacteriophage T4., Nature 227 (1970) 680–685.

[39] H. Lineweaver, D. Burk, The Determination of Enzyme Dissociation Constants, J. Am. Chem. Soc. 56 (1934) 658–666. https://doi.org/10.1021/ja01318a036.

[40] C. Tian, K. Kasavajhala, K.A.A. Belfon, L. Raguette, H. Huang, A.N. Migues, J. Bickel, Y. Wang, J. Pincay, Q. Wu, C. Simmerling, ff19SB: Amino-Acid-Specific Protein Backbone Parameters Trained against Quantum Mechanics Energy Surfaces in Solution, J. Chem. Theory Comput. 16 (2020) 528–552. https://doi.org/10.1021/acs.jctc.9b00591.

[41] A. Tomić, G. Horvat, M. Ramek, D. Agić, H. Brkić, S. Tomić, New Zinc Ion Parameters Suitable for Classical MD Simulations of Zinc Metallopeptidases, J. Chem. Inf. Model. 59 (2019) 3437–3453. https://doi.org/10.1021/acs.jcim.9b00235.

[42] S. Izadi, R. Anandakrishnan, A. V. Onufriev, Building water models: A different approach, J. Phys. Chem. Lett. 5 (2014) 3863–3871. https://doi.org/10.1021/jz501780a.

[43] R. Salomon-Ferrer, D.A. Case, R.C. Walker, An overview of the Amber biomolecular simulation package, Wiley Interdiscip. Rev. Comput. Mol. Sci. 3 (2013) 198–210. https://doi.org/10.1002/wcms.1121.

[44] H.J.C. Berendsen, J.P.M. Postma, W.F. Van Gunsteren, A. Dinola, J.R. Haak, Molecular dynamics with coupling to an external bath, J. Chem. Phys. 81 (1984) 3684–3690. https://doi.org/10.1063/1.448118.

[45] R.J. Loncharich, B.R. Brooks, R.W. Pastor, Langevin dynamics of peptides: The frictional dependence of isomerization rates of N-acetylalanyl-N'-methylamide, Biopolymers 32 (1992) 523–535. https://doi.org/10.1002/bip.360320508.

[46] J.M.J. Swanson, R.H. Henchman, J.A. McCammon, Revisiting Free Energy Calculations: A Theoretical Connection to MM/PBSA and Direct Calculation of the Association Free Energy, Biophys. J. 86 (2004) 67–74. https://doi.org/10.1016/S0006-3495(04)74084-9.

[47] M.L. Connolly, Analytical molecular surface calculation, J. Appl. Crystallogr. 16 (1983) 548–558. https://doi.org/10.1107/s0021889883010985.

[48] G. Malovan, B. Hierzberger, S. Suraci, M. Schaefer, K. Santos, S. Jha, P. Macheroux, The emerging role of dipeptidyl peptidase 3 in pathophysiology, FEBS J. (2022) 1–17. https://doi.org/10.1111/febs.16429.

[49] R. Breinbauer, J. Ivkovic, S. Jha, C. Lembacher-Fadum, J. Puschnig, P. Kumar, V. Reithofer, K. Gruber, P. Macheroux, Efficient entropy-driven inhibition of dipeptidyl peptidase III by hydroxyethylene transition state peptidomimetics, Chem. – A Eur. J. (2021). https://doi.org/10.1002/chem.202102204.

[50] J. Matić, F. Šupljika, N. Tir, P. Piotrowski, C. Schmuck, M. Abramić, I. Piantanida, S. Tomić, Guanidiniocarbonyl-pyrrole-aryl conjugates as inhibitors of human dipeptidyl peptidase III: combined experimental and computational study, RSC Adv. 6 (2016) 83044–83052. https://doi.org/10.1039/C6RA16966J.

[51] A. Hromić-Jahjefendić, N. Jajčanin Jozić, S. Kazazić, M. Grabar Branilović, Z. Karačić, J.H. Schrittwieser, K.M.P. Das, M. Tomin, M. Oberer, K. Gruber, M. Abramić, S. Tomić, A novel Porphyromonas gingivalis enzyme: An atypical dipeptidyl peptidase III with an ARM repeat domain, PLoS One 12 (2017) e0188915. https://doi.org/10.1371/journal.pone.0188915.

[52] H.B. Burgi, J.D. Dunitz, J.M. Lehn, G. Wipff, Stereochemistry of reaction paths at carbonyl centres, Tetrahedron 30 (1974) 1563–1572. https://doi.org/10.1016/S0040-4020(01)90678-7.

APPENDIX – Additional information can be found in the Supplementary data.

TABLES

Table 1. Interaction of human DPP III with neuropeptides: peptide degradation was studied using HPLC-MS, and inhibition constants K_i were measured for inhibition of human DPP III in reaction with a fluorescent substrate analogue. The peptides are sorted according to increasing K_i

peptide	sequence	cleaved[a]	K_i / µM [b]
I-tynorphin	IVYPW	Y	0.00045 ± 0.00005
S-tynorphin	SVYPW	Y	0.0077 ± 0.0007
tynorphin	VVYPW	Y	0.0112 ± 0.0008
valorphin	VVYPWTQ	Y	0.0365 ± 0.0029
β-casomorphin	YPFVEPI	Y	1.0 ± 0.1
angiotensin II	DRVYIHPF	Y	4.4 ± 0.5
Leu-valorphin-Arg	LVVYPWTQR	Y	5.2 ± 0.5
hemorphin-4	YPWT	Y	6.5 ± 0.7
endomorphin-2	YPFF	Y	10.4 ± 1.0
Leu-enkephalin	YGGFL	Y	10.4 ± 1.4
Arg-vasopressin	C*YFQNC*PRG	N	n. d. [c]
hemopressin	PVNFKFLSH	N	n. d.
β-neoendorphin	YGGFLRKYP	N	n. d.

* - denoting a disulfide bridge

[a] – cleavage (Y yes or N no) determined by HPLC-MS as reduction of peptide amount after incubation of 1 mM peptide with 0.18 µM enzyme after 24 h at 25 °C in ammonium bicarbonate buffer pH = 7.4

[b] – inhibition constant for inhibition of enzyme-catalyzed cleavage of artificial substrate Arg_2-2NA at 25 °C in 20 mM TrisHCl buffer pH = 7.5

[c] – no inhibition trend detected with peptide in the range of 1-50 µM

Table 2. Thermodynamic parameters of peptide binding to human DPP III at 25 °C and pH = 7.5 in 20 mM TrisHCl buffer.

peptide	K_d / μM	$\Delta_r H$ /kcal mol^{-1}	$\Delta_r G$ /kcal mol^{-1}	$-T^*\Delta_r S$ /kcal mol^{-1}
I-tynorphin	0.0973 ± 0.0091	8.01 ± 0.24	-9.58 ± 0.05	-17.6 ± 0.2
S-tynorphin	0.298 ± 0.061	5.69 ± 0.24	-8.91 ± 0.12	-14.7 ± 0.4
tynorphin	0.386 ± 0.127	6.19 ± 0.29	-8.77 ± 0.19	-15.0 ± 0.1
valorphin	1.78 ± 0.21	4.64 ± 0.19	-7.86 ± 0.07	-12.5 ± 0.1
angiotensin II	2.22 ± 0.24	6.17 ± 0.72	-7.72 ± 0.07	-13.9 ± 0.6
Leu-valorphin-Arg	2.50 ± 1.92	4.61 ± 2.15	-7.77 ± 0.45	-12.4 ± 1.8
hemorphin-4	39.4 ± 14.6	8.70 ± 1.82	-6.05 ± 0.24	-14.7 ± 1.6
endomorphin-2	40.1 ± 4.8			
Leu-enkephalin	118 ± 39			
β-casomorphin	130 ± 87			
Arg-vasopressin	n. d.			
hemopressin	n. d.			
β-neoendorphin	n. d.			

n.d. – binding not detected

Table 3. Kinetic parameters of peptide degradation as measured by ITC using SIM at 25 °C in 50 mM Tris-HCl buffer with 100 mM NaCl and pH = 8.0

peptide	$\Delta_r H$ / kcal mol^{-1}	K_M / µM	k_{cat} / s^{-1}	(k_{cat}/K_M) / s^{-1} M^{-1}
Leu-valorphin-Arg	-1.53 ± 0.07	33.9 ± 6.4	0.35 ± 0.09	$1.03 \cdot 10^4$
Leu-enkephalin	-1.57 ± 0.02	34.7 ± 5.7	1.08 ± 0.12	$3.11 \cdot 10^4$
hemorphin-4	-1.79 ± 0.17	55.1 ± 13.1	6.11 ± 0.96	$1.11 \cdot 10^5$

FIGURE CAPTIONS (all figures in color)

Figure 1. ITC final figures and signature plots for selected neuropeptides binding to human DPP III at 25 °C: a) Tynorphin; b) Valorphin; c) Hemorphin-4

Figure 2. The ITC SIM raw plots determined for slow substrates a) Tynorphin and b) Valorphin at 25 °C. The ITC SIM raw and rate plots for substrates c) Hemorphin-4 and d) Leu-enkephalin at 25 °C.

Figure 3. MM/PBSA energies (enthalpy contribution) for neuropeptides bound to DPP III. Energies were calculated on a set of 10 uniformly distributed 20 ns long time intervals sampled throughout 1 μs long MD simulations. The average values (± standard deviations) were calculated for 2000 frames per interval (every 10 ps). The energies of the simulations with the lowest binding enthalpies are shown.

Figure 4. Peptide (sticks with yellow coloured carbon atoms) bound to human DPP III. The same view, with N-terminus on the right, is shown for all peptides. The representative binding mode from the 20-ns long time interval with the lowest MM/PBSA free energy of binding determined during the MD simulations (Fig. 3) is shown for DPP III in complex with: a) tynorphin, b) valorphin, c) Leu-enkephalin, and e) hemorphin-4. The residues of the upper and lower protein domains that make electrostatic interactions (indicated by dashed black lines) with the peptide or are highlighted by the MM/GBSA (*vide infra*) are shown as sticks with carbon atoms coloured pink and grey, respectively. The residues of the β-strand of the lower protein domain that form hydrogen bonds with the first three residues of the N-terminus of the peptide (at the P2, P1, and P1' subsites) are shown as sticks with cyan carbon atoms. The zinc ion is shown as a green sphere. Only polar hydrogen atoms are shown.

Figure 5. The free energies of binding of neuropeptides to DPP III were calculated between the individual amino acid residues of the ligand and the whole protein. The calculations were performed using MM/GBSA for the last 0.6 μs of the MD simulations of the complexes. The amino acid residues of the peptides are denoted as P1 to Pn and P1' to Pn' (a), counting from the scissile peptide bond to the N- and C-terminus of a peptide, respectively. The total contribution of binding free energy per ligands' residues (b). The contribution of each residues side chain (SC) and backbone (BB) atoms of the residues to the total binding free energy is shown, graphs (c) and (d), respectively. The values are given for the simulations with the lowest MM/PBSA binding enthalpies (Fig. 3).

Figure 6. MM/GBSA binding free energies (± standard deviation) of each DPP III in complex with the neuropeptides calculated for amino acid residues of the protein on a set of conformers sampled during 0.6 μs (from 400th till 1000th ns) of 1 μs long MD simulations. Values are given for the simulations with the lowest binding enthalpies (Fig. 3) and for residues with energy contributions above ±1.5 kcal/mol. Ligand subsites (P1 to Pn and P1' to Pn', counting from the scissile peptide bond to the N- and C- termini of the peptides, respectively) interacting with protein residues of the lower (a) and upper (b) domain are indicated.

Figure 7. Box plots of the: a) distance between the zinc ion and the peptide carbonyl oxygen (O) atom at the P1 position, b) distance between the oxygen atom of the activated water molecule (Ow) and carbonyl carbon (C) atom at P1 position, and c) angle defining the direction of OH^- attack calculated between O-C-Ow atoms. The activated water molecule is the one that simultaneously coordinates Zn and makes hydrogen bond with E451. Values are obtained from MD simulations with the low MM/PBSA binding enthalpies. The whiskers depict one standard deviation, dashes min and max values in data set and crosses the 1st and 99th percentiles.

FIGURES

Int J Biol Macromol, Karačić et al., Figure 1.

a) Tynorphin b) Valorphin c) Hemorphin-4

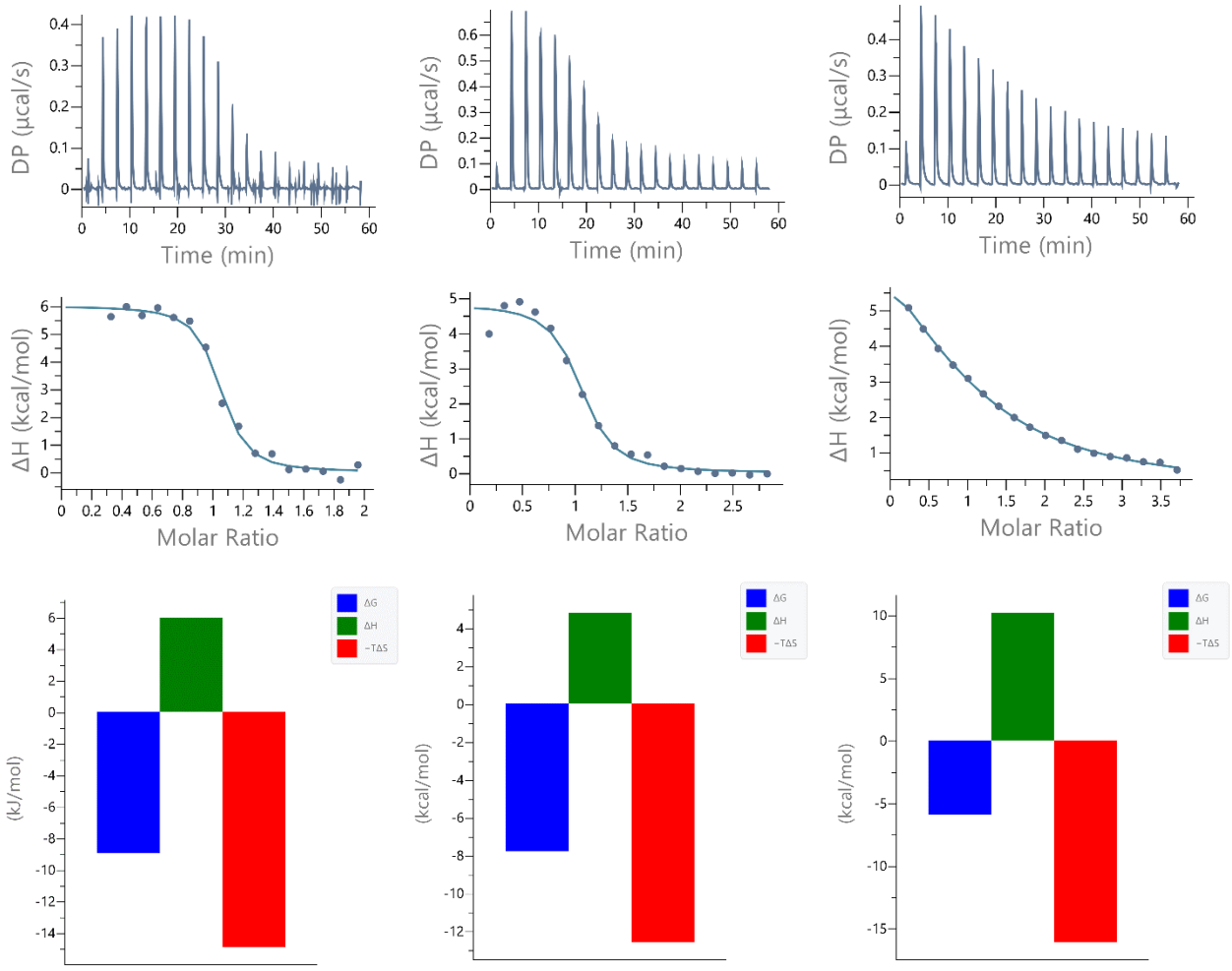

Int J Biol Macromol, Karačić et al., Figure 2.

a) Tynorphin

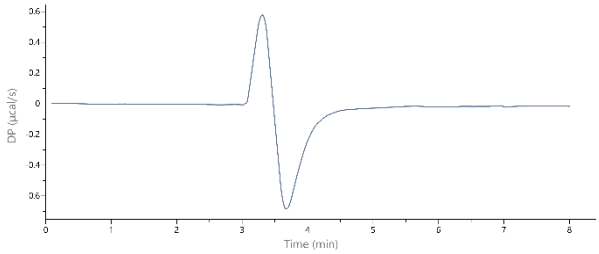

b) Valorphin

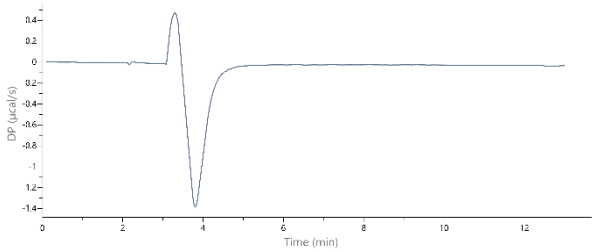

c) Hemorphin-4

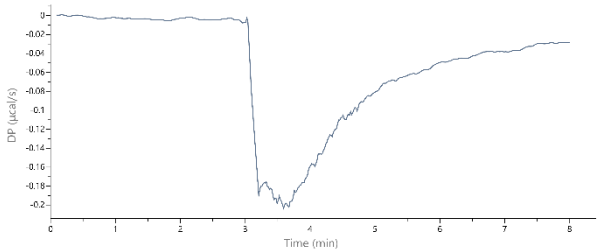

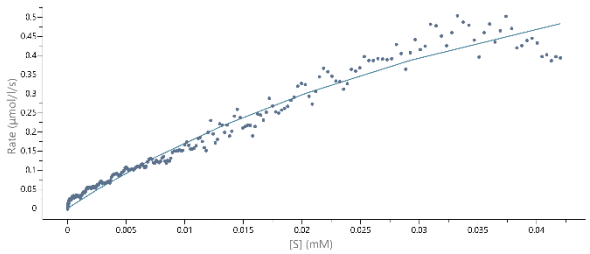

d) Leu-enkephalin

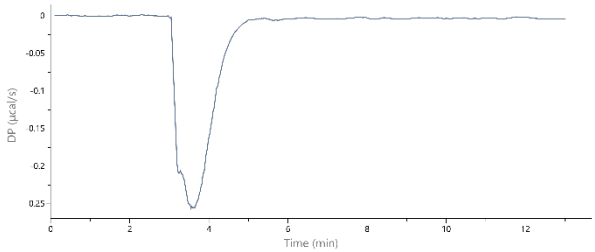

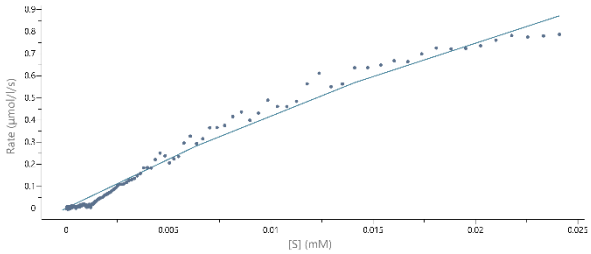

Int J Biol Macromol, Karačić et al., Figure 3.

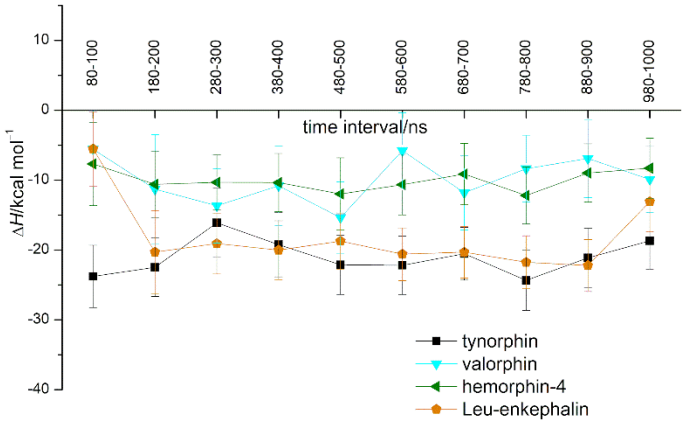

Int J Biol Macromol, Karačić et al., Figure 4.

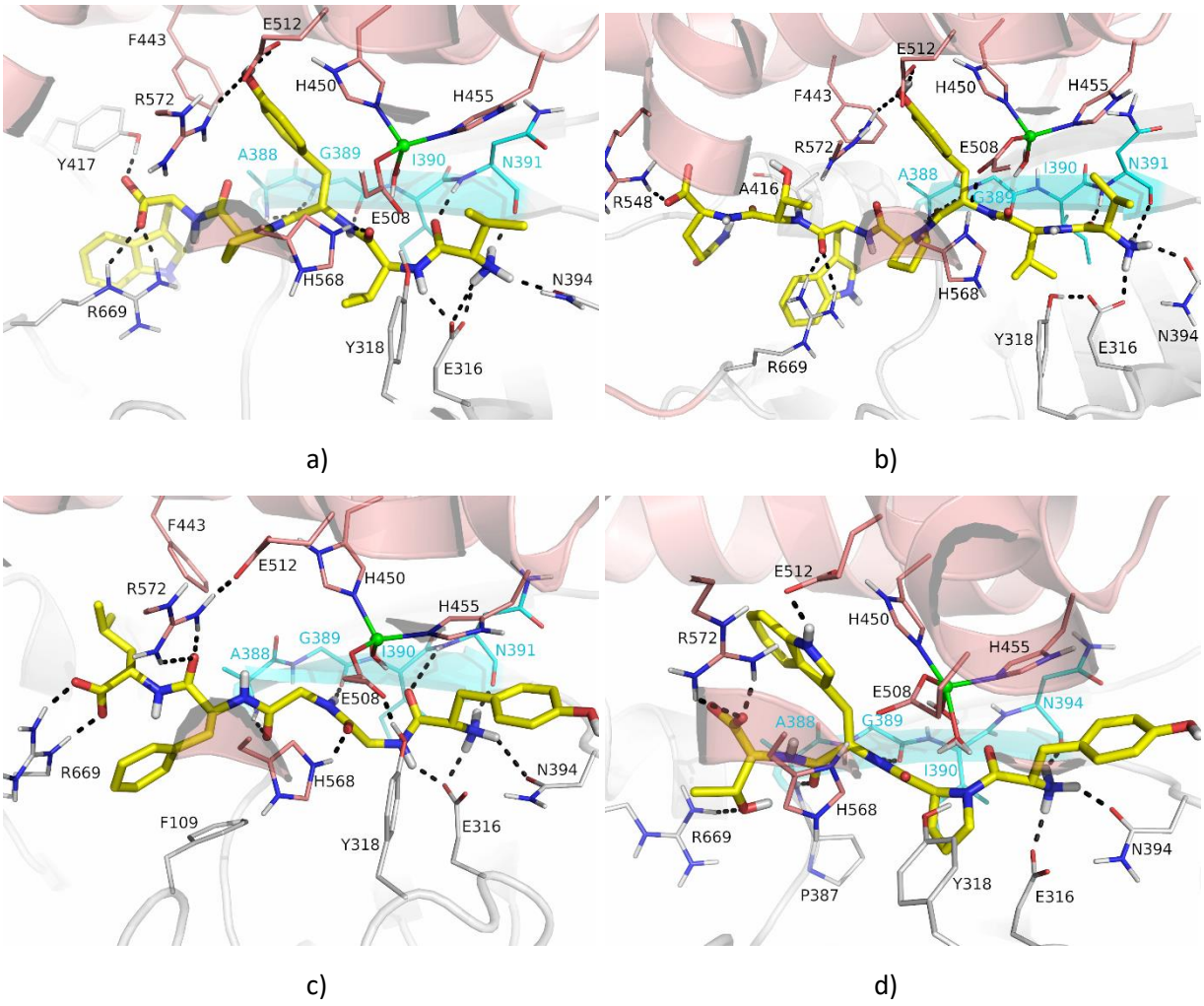

Int J Biol Macromol, Karačić et al., Figure 5.

	P2-P1-P1'-P2'-P3'-P4'-P5'						
tynorphin	V	V	Y	P	W		
valorphin	V	V	Y	P	W	T	Q
Leu-enkephalin	Y	G	G	F	L		
hemorphin-4	Y	P	W	T			

a)

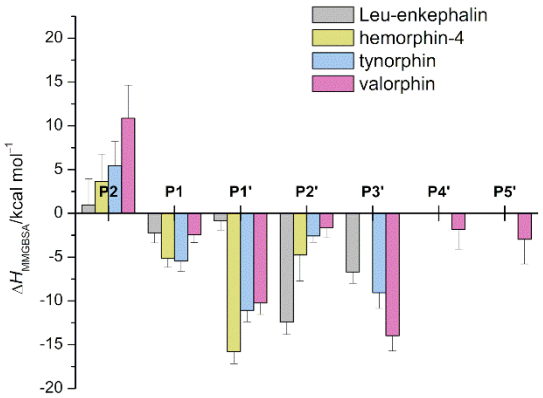

b)

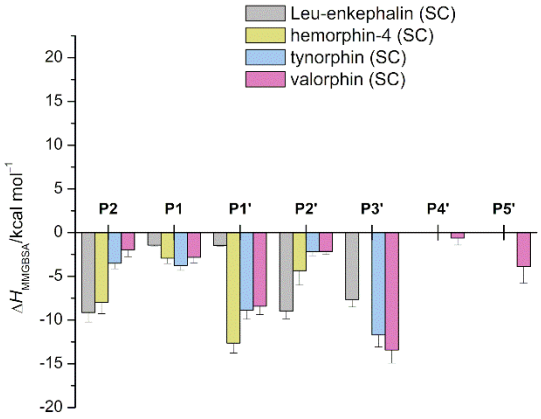

c)

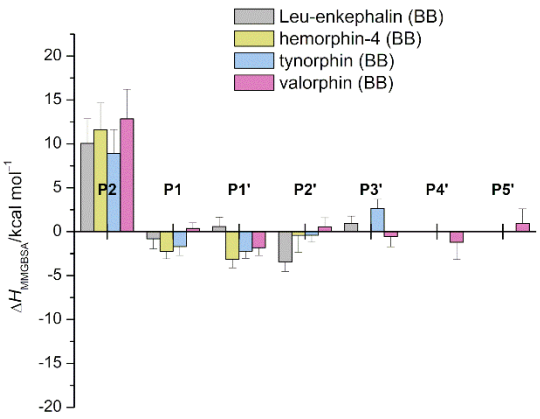

d)

Int J Biol Macromol, Karačić et al., Figure 6.

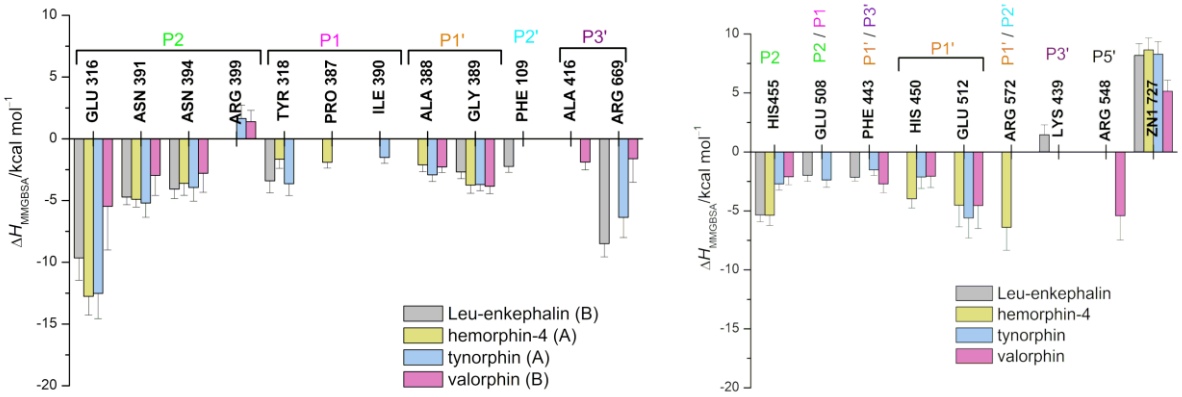

a) b)

Int J Biol Macromol, Karačić et al., Figure 7.

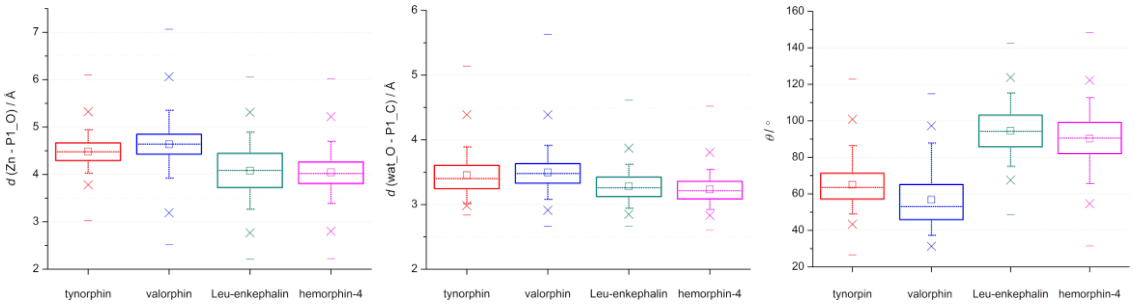

a) b) c)